In-depth study of the influence of electrolyte composition on coatings prepared by plasma electrolytic oxidation of TA6V alloy

M. Laveissière, H. Cerda, Jérôme Roche, Laurent Cassayre, Laurent Arurault

In-depth study of the influence of electrolyte composition on coatings prepared by plasma electrolytic oxidation of TA6V alloy

M. Laveissière[a], H. Cerda[a,b], J. Roche[c], L. Cassayre[d], L. Arurault[c,*]

[a] IRT Saint Exupéry, 3 Rue Tarfaya, 31400 Toulouse, France
[b] Liebherr Aerospace, 408 avenue des Etats-Unis, 31016 Toulouse Cedex 2, France
[c] CIRIMAT - Université de Toulouse, CNRS, UT3 – Paul Sabatier, 118 route de Narbonne, 31062 Toulouse Cedex 09, France
[d] Laboratoire de Génie Chimique, Université de Toulouse, CNRS, Toulouse, France

Keywords:
Titanium alloy
TA6V
Plasma electrolytic oxidation
Coating characteristics
Electrolyte species
Thermodynamic calculations

A B S T R A C T

Coatings were prepared on TA6V alloy by plasma electrolytic oxidation (PEO) using a standard electrical signal. Influence of electrolyte composition on coating characteristics was then extensively studied using four electrolytes of increasing complexity, containing KOH, Na_2SiO_3 and $NaAlO_2$. The combination of SEM, GDOES, XRD characterizations on the one hand and of thermodynamic calculations on the other hand, deeply clarified coating compositions, showing in particular that they include both amorphous and crystalline phases. Amorphous phase resulted directly from the presence of silicate in solution, and was made of complex Si-based oxides difficult to clearly identify. Depending on electrolyte composition, crystalline phases in coatings included simple oxide (i.e. anatase and rutile TiO_2) and/or mixed oxide (Al_2TiO_5), resulting from both substrate oxidation and deposition from electrolyte. Therefore, this study successfully offered an innovative approach, combining both experimental characterizations and thermodynamic calculations, to study and tune chemical characteristics of PEO coatings on TA6V.

1. Introduction

Thanks to outstanding thermal and corrosion resistance properties, titanium and its alloys uses are growing rapidly, e.g. for applications in aerospace, marine and biomedical fields. Nevertheless, their tribological properties often limit their application. Therefore, it has become essential to develop new specific coatings in order to prevent the effects of wear and friction.

Plasma electrolytic oxidation (PEO) is an innovating electrochemical process, allowing to preparing ceramic-like coatings showing promising mechanical properties. Its operating parameters, which have high influences on the prepared coating characteristics, can be divided in three groups, linked with the metal substrate, or the applied electrical signal, or the electrolytic solution. In the present study, TA6V was chosen as the substrate, while a standard electrical signal was kept unchanged.

The main aim of this work is to give a deep understanding of the influence of electrolyte composition on PEO coating characteristics.

Concerning the electrolyte, previous studies were mainly focused on the influence of the bath temperature and chemical composition. The impact of bath temperature on coating properties was studied by Habazaki et al. [1] using Ti-15V-3Al-3V-3Sn in a mixed electrolyte ($K_2Al_2O_4$, Na_3PO_4, NaOH), in the 5–40 °C temperature range. Higher is the bath temperature, more porous and rough is the coating, while coatings obtained at lower temperatures (5 and 20 °C) are more uniform and smooth. Al_2TiO_5 and γ-Al_2O_3 compounds were always present, while α-Al_2O_3 was specifically formed at 5 °C and rutile-TiO_2 at 40 °C. In the present study, bath temperature was kept constant (20 ± 2 °C) to limit the number of variables.

In previous studies, electrolytes used for the PEO treatment of titanium alloys usually include aluminates, silicates, phosphates ions, as single-component electrolyte or in mixed bath. Usually, silicate addition in the electrolyte allows obtaining coatings with higher thickness but also higher roughness and lower adhesion [2–4]. On the contrary, phosphate based electrolytes induce lower coating thicknesses and roughness, but better adhesion [3]. The electrolyte composition influences the chemical composition of the PEO coatings [2,5–7], because electrolyte compounds, especially anions, can either be directly integrated in the coating or combine with elements from the metal alloy. For instance, mixed oxides (e.g. Al_2TiO_5) are formed by substrate oxidation and integration of elements from the electrolyte [8,9]. Wang et al. [10] showed that aluminate ($NaAlO_2$) addition in the electrolyte

* Corresponding author.
E-mail address: arurault@chimie.ups-tlse.fr (L. Arurault).

https://doi.org/10.1016/j.surfcoat.2018.12.122

increases also the proportion of rutile, i.e. a hard phase of titanium oxide TiO_2, in the coating. With a mixed electrolyte including both silicates and phosphates, Li et al. [3] showed in particular the simultaneous incorporation of both compounds. Furthermore, Banakh et al. [11] demonstrated that the incorporation of phosphate and calcium, from the electrolyte {KOH + $Ca_3(PO_4)_2$}, was preferentially carried out in the coating amorphous phase. Khorasanian et al. [12] have studied a low cost and original electrolyte composed of sodium silicate, hydrogen peroxide, starch and sodium hydroxide. Resulting coatings were mainly made of rutile and anatase TiO_2 phases, and of non-stoichiometric titanium oxide, these dense coatings improving the anti-wear properties of the TA6V substrate.

The first main idea resulting from these studies is that the electrolyte composition plays a key role in composition, growth kinetics and morphology of PEO coatings, all these characteristics having a significant impact on the subsequent use properties of the coatings. The second is that two mechanisms (i.e. deposition from electrolyte and substrate oxidation) contribute to the coating growth, but sometimes compete with each other, especially when mixed electrolytes are used. The third idea is that there is a lack of knowledge about the electrolyte speciation, in relation with the chemical composition of both amorphous and crystalline phases included in PEO coatings.

To study different electrolytes and to identify the specific influence of each component on the coating characteristics, our strategy was based on the implementation of electrolytes of increasing complexity, i.e. first mono-component {KOH}, then two-components {KOH + Si} and finally tri-components {KOH + Al + Si}. For each electrolyte, coatings were extensively characterized by SEM, GDOES, XRD techniques. In addition, equilibrium calculations were carried out in order to improve our understanding of the coating formation. First, the thermodynamic equilibrium of the electrolytes was computed to evaluate the nature and the amount of the main ionic species in aqueous solution, as well as the nature of any solid phases. Second, high temperature phase diagrams were calculated in order to discuss the nature of phases that might form in the coating.

2. Experimental

2.1. Materials and electrolytes

Rectangular substrates (120 × 80 × 1 mm) made of TA6V alloy (88 wt%Ti, 6%Al, 4%V) were degreased with acetone prior to being treated by PEO. A stainless steel plate with identical dimensions was used as a counter-electrode. A standard input electrical signal (Fig. 1) was applied in all experiments using CER307-CIRTEM power supply. During PEO treatment, the electrolyte was stirred and thermostated at 20 ± 2 °C. The treated samples were then cleaned with distilled water and dried in air. In this study, KOH, $Na_2SiO_3{\cdot}5H_2O$ and $NaAlO_2$ commercial compounds were used to prepare four aqueous electrolytes, whose compositions, experimental conductivities and pH values are displayed in Table 1.

Table 1
Aqueous electrolytes composition, experimental pH and conductivity values.

Electrolyte	Composition	pH	Conductivity/mS cm^{-1}
{KOH}	0.036 M KOH	12.98	7.5
{KOH + Si}	0.036 M KOH 0.094 M Na_2SiO_3	12.96	30.0
{KOH + Al + Si (C_1)}	0.036 M KOH 0.047 M $NaAlO_2$ 0.094 M Na_2SiO_3	13.00	41.6
{KOH + Al + Si (C_2)}	0.036 M KOH 0.047 M $NaAlO_2$ 0.0094 M Na_2SiO_3	12.78	15.3

2.2. Electrolyte and coating characterizations

Electrolyte turbidity was studied using a Turbiscan LAB device (Formulaction), and the associated Turbisoft Software. Gel formed in {KOH + Al + Si (C_1)} electrolyte was characterized using solid Nuclear Magnetic Resonance spectroscopy (NMR) on a Brucker Avance 400 device; NMR spectra of 13C, 27Al and 29Si were analyzed with MNova software.

X-ray diffraction (XRD) was used to analyze both gel and coatings. XRD spectra were obtained in the 20–100° (2θ) range, with a Brucker AXS D4 ENDEAVOR device using Bragg-Brentano θ-2θ geometry with a copper anticathode (CuKα, λ = 1.541 Å). JCPDS cards used for gel characterization were 01-089-1667 (SiO_2), 01-078-0190 (KOH), 00-038-0337 ($K_2Al_2Si_3O_{10}{\cdot}2H_2O$), 00-019-1130 ($Na_2CO_3$) and 00-008-0448 ($Na_2CO_3{\cdot}H_2O$). Concerning PEO coatings, JCPDS cards 01-086-0148, 00-021-1272 and 00-041-0258, for rutile-TiO_2, anatase-TiO_2 and

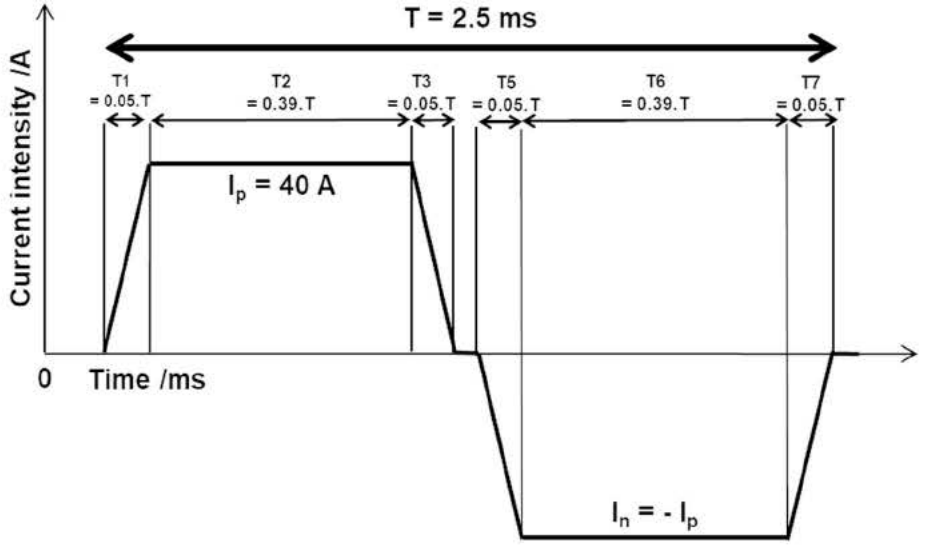

Fig. 1. Schematic representation of the input electrical waveform at a 400 Hz frequency.

Table 2
Results of equilibrium calculations for the four electrolytes.

Electrolyte	Solution species (mol L^{-1})									Solids (g L^{-1})
	pH	K^+	$KOH_{(aq)}$	OH^-	Na^+	$NaOH_{(aq)}$	$HSiO_3^-$	$H_2SiO_4^{2-}$	AlO_2^-	
KOH	12.47	3.5×10^{-2}	5.7×10^{-4}	2.9×10^{-2}						None
KOH + Si	12.84	3.5×10^{-2}	5.7×10^{-4}	6.9×10^{-2}	1.9×10^{-1}	1.6×10^{-3}	4.5×10^{-2}	2.9×10^{-2}		None
KOH + Al + Si (C_1)	13.12	4.8×10^{-3}	1.5×10^{-4}	1.3×10^{-1}	2.1×10^{-1}	3.6×10^{-3}	1.0×10^{-2}	1.2×10^{-3}	6.3×10^{-5}	9.1 ($KAlSiO_4$, $NaAlSi_2O_6{\cdot}nH_2O$)
KOH + Al + Si (C_2)	12.62	2.6×10^{-2}	2.9×10^{-4}	4.2×10^{-2}	6.4×10^{-2}	3.8×10^{-4}	8.3×10^{-7}	2.5×10^{-7}	3.7×10^{-2}	1.5 ($KAlSiO_4$)

Al_2TiO_5 respectively, were used. Crystalline phase proportions were determined using the Reference Intensity Ratio method, while crystallite size was calculated with Scherrer formula.

Coating thickness was measured using an Eddy current device (Dualscope FMP20 - Fisher), ten measurements being performed on each sample. Arithmetic roughness S_a, was obtained using optical profilometry (S-Neox, Sensofar), according to ISO 25178. Cross-sectional views of the coatings were performed by Scanning Electron Microscopy (SEM-JEOL JSM-6510LV) after a silver-metallization (JEOL JFC 1200 Fine Coater). Additional Energy Dispersive X-ray Spectrometry (EDS) mappings were performed using Princeton Gamma Tech Spirit device. Coating composition was also characterized with Glow Discharge-Optical Emission Spectroscopy (GDOES) technique with a Go Profiler 2 (Horiba Scientific).

2.3. Thermodynamic calculations

Equilibrium calculations were carried out for each of the electrolytes. The main features of the thermodynamic model are as follows:

- The liquid aqueous phase is described according to an activity coefficient model (modified Debye-Hückel using B-dot equation), which requires a single parameter for each compound. This approach is justified by the intermediate ionic concentrations of the electrolytes (maximum ionic strength of about 0.5).
- All solid phases are considered as stoichiometric compounds (no miscibility between compounds). Each compound having a saturation index superior to zero forms a solid phase in equilibrium with the aqueous phase (i.e. no supersaturation of the aqueous solution is allowed).
- No gas phase is considered in the model.

The calculations are performed with the PHREEQC software [13], and all model parameters (equilibrium constants and Debye-Hückel parameters for aqueous species) come from the 2017 version of the Thermoddem database [14]. For each electrolyte, the input is the molar concentration of each additive, the temperature (20 °C) and the pressure (1 atm). The calculation output provides the concentration of each solution species (anions, cations and neutral species), from which the pH is derived, as well as the amount and nature of the solid phases if present.

In addition to these calculations specific to the aqueous medium, high temperature equilibria were computed for the two binary oxide systems TiO_2-Al_2O_3 and TiO_2-SiO_2. The phase diagrams are calculated using the FactSage 7.2 software [15] and the FToxid database, which includes models of the thermochemical properties of the oxide phases in Ti-Al-O [16] and Ti-Si-O [17] systems.

3. Results and discussion

3.1. Single-component electrolyte {KOH}

The first electrolyte studied is a single-component electrolyte (noted {KOH}), which contains only potassium hydroxide, at a concentration of 2 g L^{-1} (3.6×10^{-2} mol L^{-1}). For this first electrolyte, the experimental values of electrical conductivity and pH are 7.5 mS cm^{-1} and 12.98 respectively (Table 1), the simulated pH value being 12.47 (Table 2). Concerning PEO process, small orange sparks appear on the surface of the substrate after 10 min of treatment.

Coatings prepared in this electrolyte are thin, their thicknesses do not exceed 9 µm after 50 min of treatment (Fig. 2). In addition, these coatings are 2.5 times rougher than the uncoated TA6V, their roughness (S_a) being 2.1 ± 0.1 µm, compared to 0.7 ± 0.1 µm for the bare TA6V substrate. Cross-sectional SEM views (Fig. 3a) confirm these small thicknesses and these significant roughnesses, while both cross-sectional and surface SEM views (Figs. 3 and 4) reveal a complex porosity.

Fig. 5 shows GDOES profiles in the coating prepared in {KOH} electrolyte, its roughness (S_a) having previously been reduced to 0.8 µm by manual mechanical polishing. Fig. 5 confirms, on one hand, that Ti, Al and V elements are present in the substrate, their profiles being stable for an erosion time greater than 120 s. On the other hand, the interface between the coating and the substrate does not appear precisely on the GDOES profiles; it is located between 50 and 100 s of erosion. This inaccuracy to rigorously detect the coating/substrate

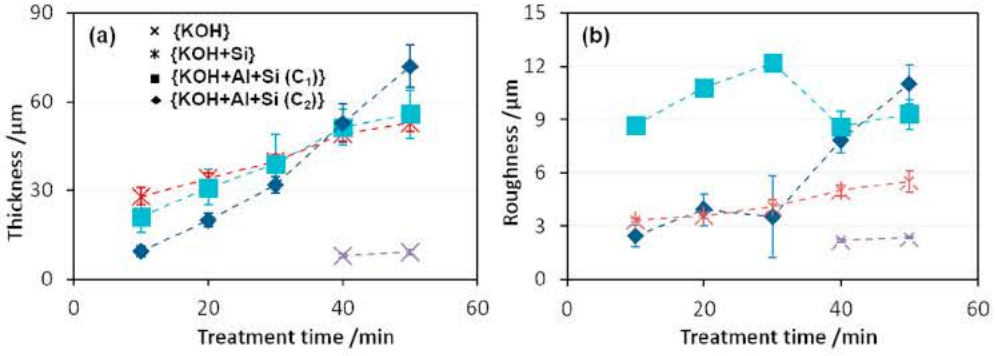

Fig. 2. Evolution of coatings (a) thickness and (b) roughness with treatment time in different electrolytes: {KOH} in purple; {KOH + Si} in red; {KOH + Al + Si (C_1)} in light blue; {KOH + Al + Si (C_2)} in dark blue. (For interpretation of the references to color in this figure legend, the reader is referred to the web version of this article.)

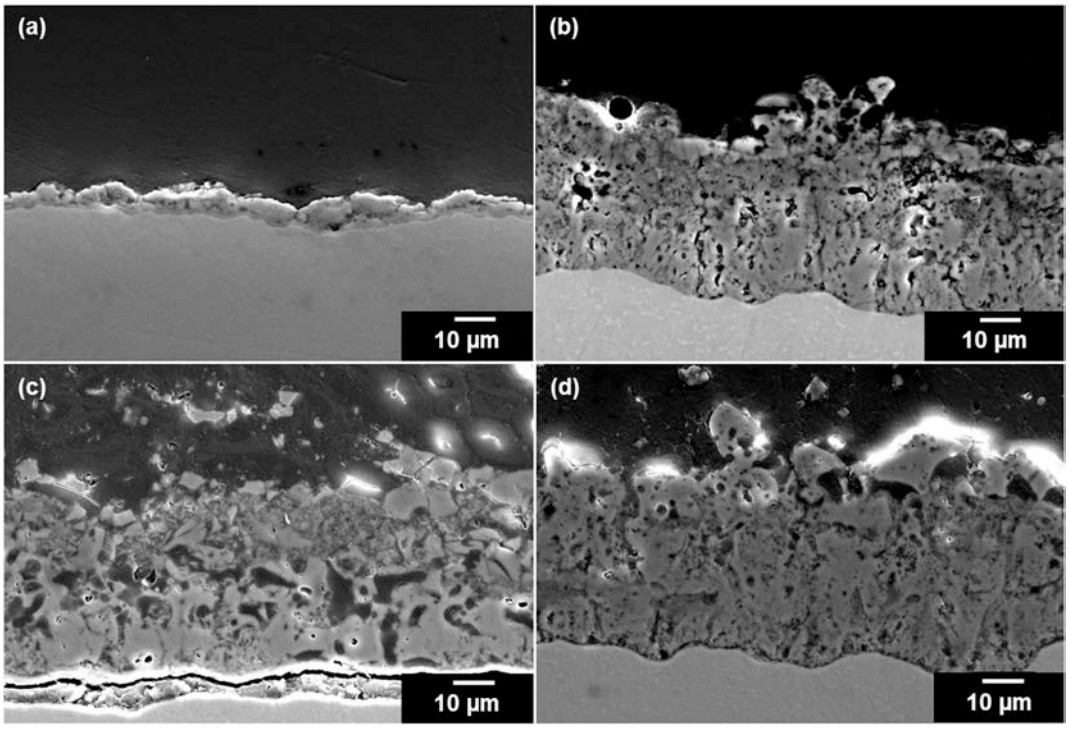

Fig. 3. SEM cross section views of PEO-treated TA6V plates in different electrolytes: (a) {KOH}; (b) {KOH + Si}; (c) {KOH + Al + Si (C_1)}; (d) {KOH + Al + Si (C_2)}.

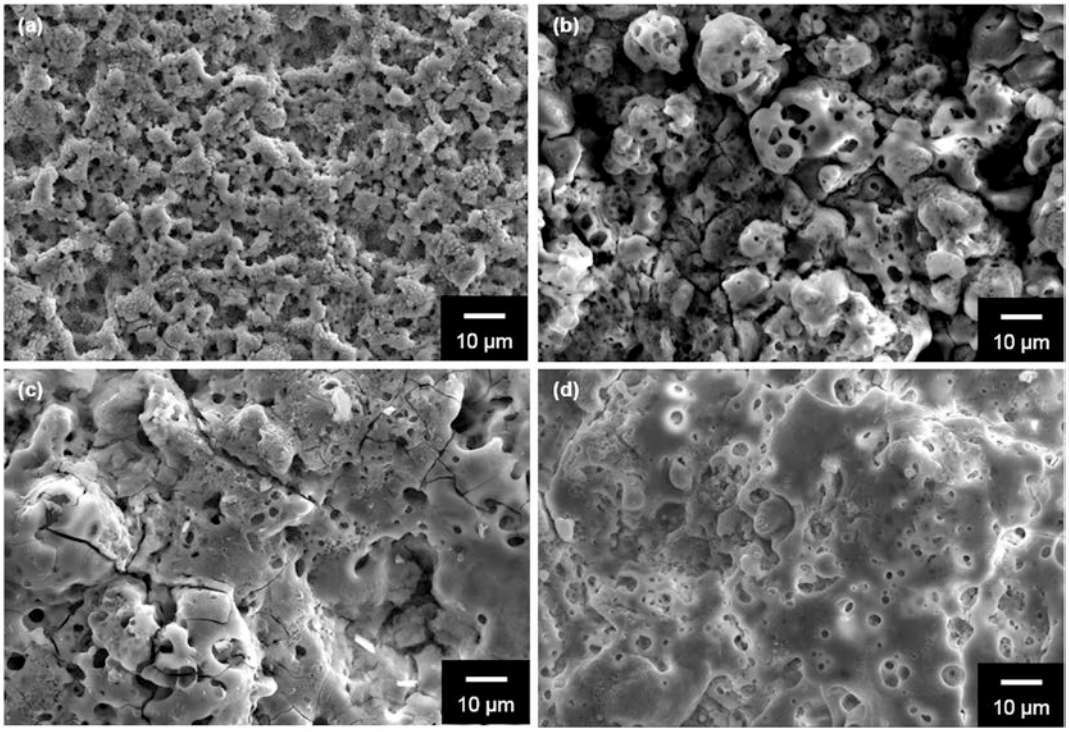

Fig. 4. SEM surface views of PEO-treated TA6V plates in different electrolytes: (a) {KOH}; (b) {KOH + Si}; (c) {KOH + Al + Si (C_1)}; (d) {KOH + Al + Si (C_2)}.

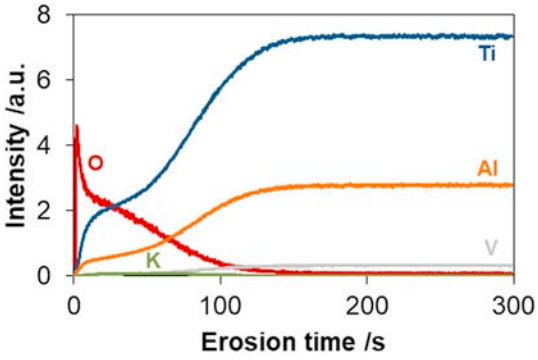

Fig. 5. GDOES depth profiles of PEO coating prepared in {KOH} electrolyte with an applied current of 40 A and treatment time of 50 min.

interface may be due to the coating roughness (0.8 μm) but also to GDOES technique itself. Concerning the coating (i.e. between 0 and 50 s), oxygen, as well as titanium and aluminium are detected, the concentrations of the last two increasing when approaching the TA6V substrate. GDOES analysis also shows the presence of very low content of potassium, while vanadium is absent. Figs. 6 and 7 present respectively the raw and analyzed X-ray patterns of the uncoated TA6V substrate and of the coating prepared in {KOH} electrolyte. Peaks associated with TA6V substrate (noted "T"), as well as with two phases (anatase "x" and rutile "+") of titanium dioxide TiO_2 can be identified (Fig. 7), relative intensity ratio of anatase and rutile being close to 44% and 56% respectively.

The formation of titanium dioxide results from the electrochemical oxidation of the titanium contained in the TA6V substrate, most likely according to the following reactions:

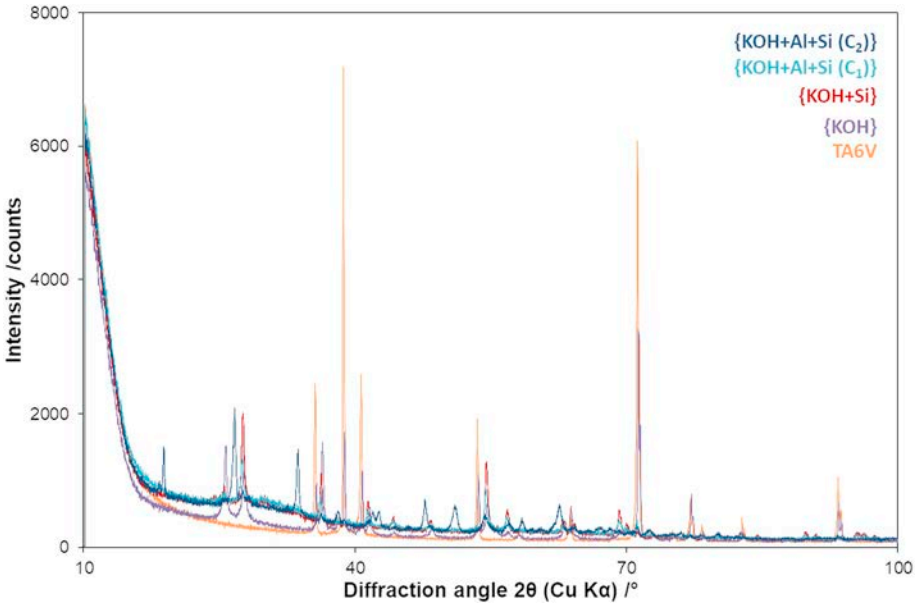

Fig. 6. Raw XRD-pattern of PEO-layers produced in different electrolytes with an applied current of 40 A and treatment time of 50 min.

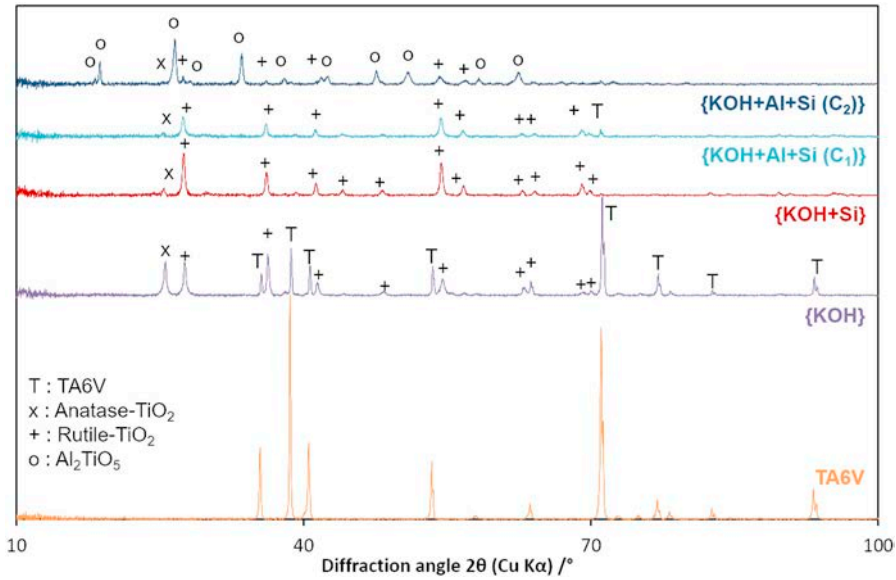

Fig. 7. Analyzed XRD-pattern of PEO-layers produced in different electrolytes with an applied current of 40 A and treatment time of 50 min.

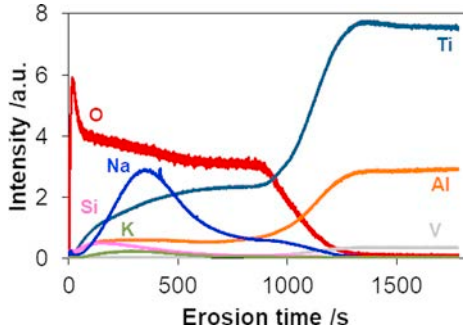

Fig. 8. GDOES depth profiles of PEO coating prepared in {KOH + Si} electrolyte with an applied current of 40 A and treatment time of 50 min.

$$Ti \rightarrow Ti^{4+} + 4e^{-} \quad (1)$$

$$Ti^{4+} + 2H_2O \rightarrow TiO_2 + 4H^{+} \quad (2)$$

$$Ti^{4+} + 2OH^{-} \rightarrow TiO_2 + 2H^{+} \quad (3)$$

The presence of both anatase and rutile phases provides essential information on surface temperatures and mechanisms, occurring during the PEO treatment. Indeed, Smith et al. [18] have shown that the transformation from bulk anatase to bulk rutile is thermodynamically favorable at all temperatures between 0 and 1100 °C, indicating that bulk anatase does not have a thermodynamic stability field. Rutile, however, is metastable with respect to anatase when the TiO_2 particle size is below roughly 14 nm. This implies that PEO first induces the formation of nanosized anatase grains, which transform into larger rutile grains because of the high temperature prevailing on the surface of the substrate.

Moreover, it should be noted that the coatings do not seem to contain other metastable titanium oxides (TiO, Ti_2O_3, TiO_3), which were nevertheless potentially conceivable [19,20]. X-ray patterns (Fig. 7) do not reveal either crystalline compounds comprising aluminium or vanadium, which are nevertheless the two main alloying elements of the substrate. GDOES analysis (Fig. 5) confirms the absence of vanadium and, in contrast, the presence of aluminium in the coating. This is likely to result from the electrochemical oxidation of the substrate (Eq. (4)) [20] and the possible subsequent formation of an amorphous phase.

$$Al \rightarrow Al^{3+} + 3e^{-} \quad (4)$$

As for the minor presence of potassium in the coating, it could result from its incorporation from the electrolyte {KOH}, which contains, according to the PHREEQC simulation, K^+ ion at a concentration of 3.5×10^{-2} mol L^{-1} (Table 2).

Considering the small thicknesses (6 to 9 µm) of the coatings produced in {KOH} electrolyte, it seems worthwhile to thicken the coatings by promoting other crystallization mechanisms and by allowing in particular the incorporation of other elements from the electrolyte into the coatings. As the literature has shown that addition of silicon-based compounds to the electrolytic bath significantly increases coating thicknesses, this strategy was envisaged for the second electrolyte, denoted as {KOH + Si}.

3.2. Bi-component electrolyte {KOH + Si}

The bi-component electrolyte {KOH + Si} was prepared by adding sodium silicates ($Na_2SiO_3{\cdot}5H_2O$ at $C_1 = 20$ g L^{-1} (i.e. 9.4×10^{-2} mol L^{-1})) to the previous electrolytic bath comprising potash (KOH), at a concentration of 2 g L^{-1} (i.e. 3.6×10^{-2} mol L^{-1}). The experimental conductivity then increased from 7.5 to 30 mS cm^{-1}, while the measured pH remains alkaline at a value of 12.96 (Table 1), the simulated pH value being 12.84 (Table 2).

In this second case, sparks are initiated from the start, continue until the end of the treatment, and are numerous and well distributed on the surface of the substrate. However, their light intensity, low at the beginning of the treatment, seems to increase slightly until reaching a maximum after approximately 15 min of treatment. Fig. 2a firstly shows a significant increase in the coating thickness, compared with those obtained in {KOH} bath. Moreover, in this two-component electrolyte, the thickness seems proportional to the treatment time, ranging from 25 to 53 µm. Concomitantly, a strong increase of the coating roughness is observed (Fig. 2b), ranging from 3 to 6 µm in the {KOH + Si} electrolyte, compared to about 2 µm, after the treatment in {KOH} bath. To summarize, the longer the treatment time, the greater the thickness and roughness. Cross-sectional SEM views (Fig. 3b) corroborate the formation of a coating that is both porous and rough, while EDS mappings (not shown) attest the presence of the elements Ti, Al, O, Si within the coating.

Fig. 8 shows GDOES profiles for the coating obtained in {KOH + Si} electrolyte. The interface between the coating and the substrate is again difficult to identify precisely; it may correspond to the beginning of the vanadium detection, this element being absent up to 900 s (in the coating), then increases from 900 to 1400 s (at the interface), and finally stabilizes thereafter (in the substrate). It should be noted that the erosion time (900–1400 s), necessary to reach this interface, is longer than the previous one (50–100 s) corresponding to the coating prepared in {KOH} electrolyte. This result can be explained by a thicker coating, i.e. 37 µm in {KOH + Si}, instead of 3 µm at most in {KOH}.

In the coating, the oxygen content decreases as the erosion time increases. Conversely, aluminium and titanium concentrations increase and then stabilize once the coating has been completely eroded and the substrate is reached. Potassium, silicon and sodium are also identified in the coating, their concentration profiles decreasing as the coating is eroded. Sodium distribution in the coating appears to be the most singular since its content is greater in the coating than at the extreme surface or near the interface.

Raw XRD results (Fig. 6) clearly show a difference in the baseline of the pattern corresponding to the coating produced in the {KOH + Si} electrolyte, this hump being attributed to the significant presence of an amorphous phase. By reporting the XRD pattern to the baseline (Fig. 7), a single peak associated with the TA6V substrate appears, while the anatase and rutile phases of the titanium oxide are again identified. The respective proportions (13 and 87%) of these two crystalline phases (anatase and rutile) are, however, different from those obtained (44 and 56%) in the {KOH} electrolyte. XRD pattern also allows calculating an average crystallites size present in the PEO coatings. For the coatings elaborated in the {KOH + Si} electrolyte, crystallites are very fine, their diameters ranging, depending on processing time, from 21 to 40 nm and from 67 to 85 nm for the TiO_2-anatase and TiO_2-rutile phases respectively. This result is in full agreement with the knowledge already mentioned, namely that anatase is stable only in the form of fine

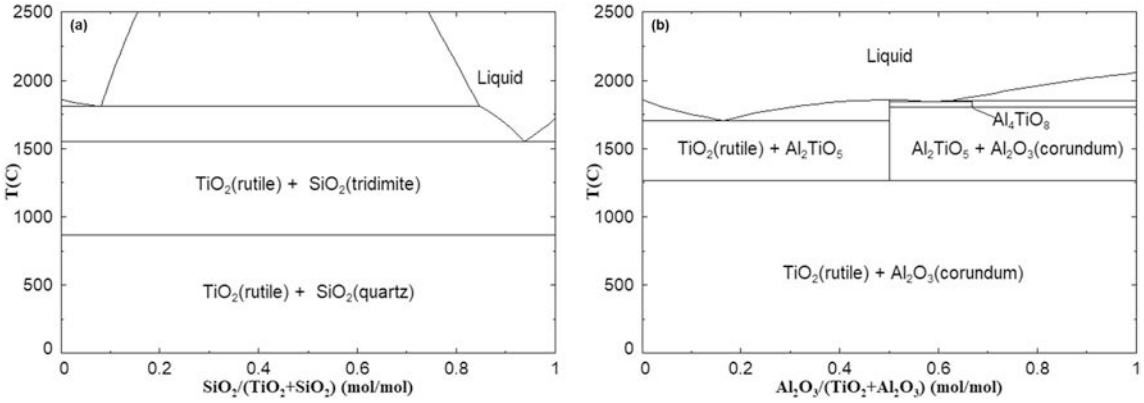

Fig. 9. Phase diagrams of (a) TiO_2-SiO_2 and (b) TiO_2-Al_2O_3 systems.

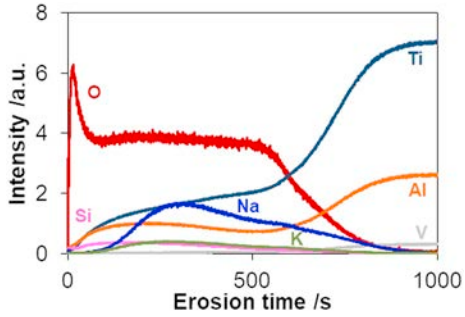

Fig. 10. GDOES depth profiles of PEO coating prepared in {KOH + Al + Si (C_1)} electrolyte with an applied current of 40 A and treatment time of 50 min.

particles (below roughly 14 nm), while rutile prevails at larger grain sizes and high temperature [18]. These small diameter values also explain why the crystallites are not detectable on SEM images and associated EDS mappings (not shown).

The results thus confirmed that the addition of silicates in the bath significantly increases coating thickness, as previous studies [2–4,12] have pointed out. The addition of sodium silicates in the electrolyte induces the existence of different anions in solution (Table 2) that are incorporated in the coating during the treatment, which is attested by GDOES analysis (Fig. 8). In particular, the presence of $HSiO_3^-$, $H_2SiO_4^{2-}$ ions might allow the formation of SiO_2-containing phases in the coating (and especially on its surface), according to the following reactions:

$$2H_2O \rightarrow O_2 + 4H^+ + 4e^- \quad (5)$$

$$HSiO_3^- + H^+ \rightarrow SiO_2 + H_2O \quad (6)$$

$$H_2SiO_4^{2-} + 2H^+ \rightarrow SiO_2 + 2H_2O \quad (7)$$

The absence of silicon compounds (oxides in particular) on the XRD pattern (Fig. 7), mean that this element has integrated an amorphous phase. This result would imply also that the interfacial temperature was below 1723 °C, i.e. the crystallization temperature of silica SiO_2 [21]. The absence of crystalline silica (SiO_2) could also be explained [22], by a hot SiO_2 redissolution (at 1400 °C) in an alkaline medium (Eq. (8)).

$$SiO_2 + 2NaOH \rightarrow Na_2SiO_3 + H_2O \quad (8)$$

According to the phase diagram (Fig. 9a), there is no mixed oxide compounds in the TiO_2-SiO_2 system. However, Na_2O and K_2O are classic additives for the preparation of SiO_2 glass, and ions of these two elements are present at high concentration in the electrolyte. Given the respective GDOES profiles for potassium and sodium (Fig. 8), the amorphous phase formed in the outside part of the coatings is thus likely to be a SiO_2-K_2O-Na_2O glass phase, even if experimental evidence of such phase is difficult to provide due to analytical difficulties.

This incorporation of elements from {KOH + Si} electrolyte in the coating, is very interesting from the point of view of its thickening. However, it would also be advantageous to form additional crystalline compounds (for example Al_2TiO_5 and Al_2O_3) within the coatings, in order to increase for instance the mechanical properties thereof. However, results have shown so far that the amount of aluminium in the TA6V substrate is not sufficient to induce the formation of simple (Al_2O_3) or mixed (Al_2TiO_5) aluminium oxides. To promote the formation of such oxides, it would therefore be beneficial to add aluminates and thus prepare a tri-component electrolyte {KOH + Al + Si (C_1)}.

3.3. *Tri-component electrolyte {KOH + Al + Si (C_1)}*

The tri-component electrolyte was prepared on the basis of the previous two-component bath, to which was added sodium aluminate at a concentration of 3.8 g L^{-1} (4.7×10^{-2} mol L^{-1}). This third electrolyte has an electrical conductivity equal to 41.6 mS cm^{-1} and an experimental pH of 13.00 (Table 1), the simulated pH being 13.12 (Table 2). It is important to note that, following the addition of aluminates in the electrolytic bath, it becomes white and turbid, whereas the previous electrolytes, {KOH} and {KOH + Si}, were translucent. Because of the bath opacity, the sparks phenomenon could not be observed in this electrolyte.

The morphological characterizations show that the coatings are as thick as those obtained in {KOH + Si} electrolyte, but are on the other hand much rougher (Fig. 2b). SEM views also reveal a porosity that does not seem significantly different from that of the previous coatings (Fig. 3c).

GDOES analysis (Fig. 10) reveals a coating/substrate interface for an erosion time between 600 and 900 s, i.e. longer than the one corresponding to the coating elaborated in {KOH} (50–100 s), but shorter than the one associated with the coating elaborated in {KOH + Si}

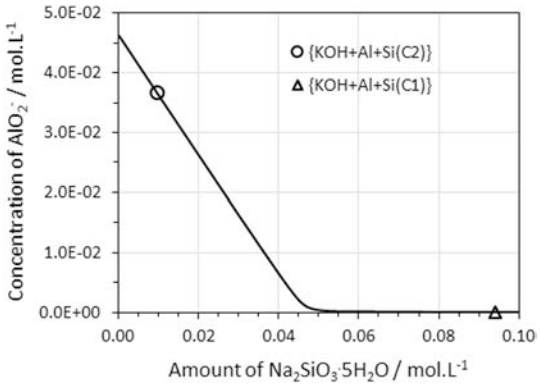

Fig. 11. Calculated evolution of the concentration of AlO_2^- species in the electrolyte with the amount of $Na_2SiO_3{\cdot}5H_2O$ in an initial mixture of 0.036 M KOH + 0.047 M $NaAlO_2$.

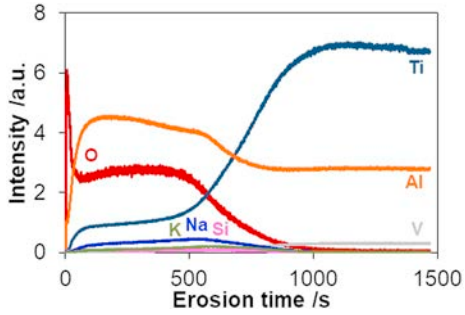

Fig. 12. GDOES depth profiles of PEO coating prepared in {KOH + Al + Si (C_2)} electrolyte with an applied current of 40 A and treatment time of 50 min.

(900–1400 s). GDOES profiles of sodium, silicon and potassium (from the bath), and titanium and vanadium (from the substrate) elements are almost identical to those (Fig. 8) obtained for the coating developed in {KOH + Si}. Aluminium content is higher since the specific intensity is about 1 a.u. (arbitrary unit) while it is only 0.5 a.u. in the coating elaborated in {KOH + Si} electrolyte.

On raw diffractogram (Fig. 6), the presence of an amorphous phase was highlighted, while on the analyzed X-ray pattern (Fig. 7), peaks corresponding to the TA6V substrate have almost disappeared and mainly the two TiO_2 isomorph anatase and rutile are identified. The proportions of the anatase and rutile phases are 16 and 84% respectively, i.e. values close to those obtained (13 and 87%) by using {KOH + Si} electrolyte. No crystalline structure including either aluminium or silicon can be evidenced.

The aluminium present in the coating comes partly from the TA6V substrate and partly from the aluminates of the electrolyte, these two simultaneous contributions inducing a higher content than the previous one. Since aluminium did not form any crystallized phase, the precise nature of the amorphous Al-containing compounds is difficult to determine.

However, these results can be related to empirical observations of precipitation/decantation phenomena observed in the bath (Appendix A.1) and to the formation of a gel on the samples surface during the PEO treatment. Additional characterizations (Appendix A.2) of solid-state Nuclear Magnetic Resonance (NMR) and X-ray diffraction (XRD) were performed on the gel. NMR analysis shows that the undried gel is an alumino-silicate compound having Si—Al and Si—Si—Al bonds, while the XRD analysis shows that the dried gel (at 80 °C in an oven under air) includes $K_6Si_3O_9$, SiO_2 and KOH but also $K_2Al_2Si_3O_{10}$.These characterizations are in rather good agreement with equilibrium calculations. Indeed, modelling using PHREEQC software indicates the presence of tiny amounts of aluminium ions in the aqueous phase (around 6×10^{-5} mol L^{-1}) and the precipitation of large amounts of alumino-silicate phases, i.e. $KAlSiO_4$ and $NaAlSi_2O_6{\cdot}nH_2O$ (Table 2).

In order to avoid these phenomena of formation and precipitation of such gel, as well as to increase free aluminium ions content in solution to promote the formation of aluminium oxides in the coating, silicate concentration was subsequently decreased. The choice of silicate concentration was driven by equilibrium calculations. Indeed, as illustrated in Fig. 11, an initial silicate concentration divided by 10 ($C_2 = 2$ g $L^{-1} = 9.4 \times 10^{-3}$ mol L^{-1}) should lead to a large amount of aluminate ions in the electrolyte.

3.4. Tri-component electrolyte {KOH + Al + Si (C_2)}

This fourth electrolyte {KOH + Al + Si (C_2)} includes the same compounds as the previous one {KOH + Al + Si (C_1)}, but with a sodium silicate concentration ($Na_2SiO_3{\cdot}5H_2O$) of $C_2 = 2$ g L^{-1} (9.4×10^{-3} mol L^{-1}) compared with $C_1 = 20$ g L^{-1} (9.4×10^{-2} mol L^{-1}). This silicate concentration decrease (by a factor of ten) leads to a lower bath conductivity, the experimental value being 15.3 mS cm^{-1} (compared with 41.6 mS cm^{-1} in {KOH + Al + Si (C_1)}). The experimental pH remains alkaline (pH = 12.78) (Table 1), while the simulated value is 12.62 (Table 2). From the process point of view, sparks become visible after about 20 min of treatment and persist until the treatment is stopped. Moreover, during the treatment, the bath remains translucent and no gelation or precipitation is visible, neither in the bath nor on TA6V surface. In this fourth electrolyte, coating thicknesses vary between 5 and 45 µm (Fig. 2). At similar elaboration time, thickness and roughness are lower in this case, in comparison with the values obtained in the previous electrolyte {KOH + Al + Si (C_1)}, except for long treatment times (40 and 50 min.).

On the basis of vanadium GDOES profile (Fig. 12), the coating/substrate interface appears for an erosion time between 600 and 900 s, i.e. a value similar to those obtained in the preceding electrolyte {KOH + Al + Si (C_1)}. In comparison with previous GDOES profiles (Fig. 10), the elements Ti, Si, K, O and especially Na are at lower concentrations in the coating, whereas on the contrary aluminium content is higher. Indeed, the specific intensity of aluminium is about 4.5 a.u. in this coating, whereas it was only about 1 a.u. in the coating obtained in {KOH + Al + Si (C_1)} electrolyte.

On XRD pattern (Fig. 7), three crystallized phases appear: the usual anatase and rutile (TiO_2) phases, but also Al_2TiO_5 mixed oxide. In addition, no allotropic phase of alumina (Al_2O_3) is identified, while a significant amorphous phase is present. Comparison of simulated species (Table 2) in the last two electrolytes, shows that concentrations of $HSiO_3^-$ and $H_2SiO_4^{2-}$ ions were divided by about 12,000 and 5000 respectively, while AlO_2^- concentration is more than 500 times higher. Moreover, contrary to the preceding electrolyte (Table 2), a single precipitate ($KAlSiO_4$) is identified in {KOH + Al + Si (C_2)} electrolyte, and its amount is much less significant (1.5 instead of 9.1 g per liter of solution).

Therefore, the reduction of silicate concentration (from $C_1 = 20$ g L^{-1} to $C_2 = 2$ g L^{-1}) allows to avoid the formation and

precipitation of alumino-silicate gel within the bath, but also to prevent silicon incorporation into the coating. As a consequence, aluminium incorporation from the abundant AlO_2^- ions in solution (Table 2) leads to the formation of Al_2TiO_5 mixed oxide. According to the TiO_2-Al_2O_3 phase diagram (Fig. 9b), the presence of this oxide indicates that crystallization temperature of elements is comprised between 1250 and 1800 °C, which is the temperature range of Al_2TiO_5 stability.

In this study, aluminates available in the bath allowed the formation of Al_2TiO_5 compound by combining titanium element from the substrate TA6V (Eqs. (1) to (3)) and elements from the electrolyte, i.e. oxygen and aluminium. Our results showed that Al_2TiO_5 formation could not be achieved only from the aluminium contained in the TA6V substrate, probably because of its too low content (6% by mass). Indeed, for a TiAl alloy, having 48 at% of aluminium, Li et al. [23] identified crystallized Al_2TiO_5 phase in the coating. Furthermore, unlike the Habazaki study [1], crystallized alumina did not form in our tests. According to the phase diagram (Fig. 9b) and the present results, higher concentrations of aluminate in the electrolyte might probably induce the formation of alumina during PEO treatment of TA6V.

4. Conclusion

Using a standard electrical signal, characteristics of coatings prepared by PEO process on TA6V alloy depend on two main competitive reaction mechanisms, i.e. substrate oxidation and deposition from electrolyte. The respective influence of four different types of electrolytes, including different concentrations of potash, aluminate and silicate, was studied. The combined approach of coating characterizations and thermodynamic calculations applied to the electrolyte and the coating, highlighted that:

- Both anatase and rutile crystalline phases of titanium oxide, are present in the coatings regardless of the composition of the electrolyte, since they result of the substrate oxidation. Because of the respective stability of these isomorphs, it is likely that anatase crystallizes in the form of nanocrystals, which gradually transform into rutile under the effect of local temperature.
- Proportion of amorphous phase in the coating is all the more important as the concentration of silicates is high in solution, this silicon incorporation in the coating being associated with a high content of the Na^+ counterion.
- A high C_{Si}/C_{Al} ratio in the electrolyte leads to the formation, in solution and at the coating surface, of an alumino-silicate gel. Its precipitation and decantation induces a destabilization of the highly silicated electrolyte, incompatible with a long and extended use.
- At a low C_{Si}/C_{Al} ratio, the formation of Al_2TiO_5 mixed oxide occurs from the aluminate ions, and not from aluminium included in the titanium substrate, as alloying element.
- In these operating conditions, alumina was not formed, despite the thermodynamic potentiality.
- Finally, it seems preferable for future wear applications, on the one hand to remove the silicates in solution in order to limit the presence of a soft amorphous phase in the coating, and on the other hand to form hard crystalline phases, such as TiO_2 and Al_2TiO_5. But it could be also interesting to improve superficial mechanical properties of TA6V alloy by promoting corundum formation through new electrolytes or optimization of the process electrical parameters.

Acknowledgments

These results were obtained under the research project “SURFINNOV” at the IRT Saint Exupéry. Authors thank the “Commissariat Général à l'Investissement” and the “Agence Nationale de la Recherche” for their financial support in the “Programme d'Investissement d'Avenir” (PIA).

Appendix A

A.1. Electrolytic bath instability

To highlight precipitation phenomena occurring in the {KOH + Al + Si (C_1)} solution, turbidity analyses were performed as a function of time, without solution stirring. Fig. A.1 shows the evolution of light transmission through this freshly prepared electrolyte, just after stirring (t_0) and after 60 min (t_0 + 60 min). At t_0, the solution is entirely cloudy and light transmission is lower than 5%. After 60 min, the lower part of the sample is still turbid (3% of light transmission), while the upper part becomes clear (89% of light transmission). Knowing that 89% of light is transmitted in deionized water, this modification of light transmission in the {KOH + Al + Si (C_1)} electrolyte clearly shows the sedimentation phenomenon, correlated with alumino-silicates solid compounds identified by PHREEQC computation. Nevertheless, this sedimentation phenomenon was not detected during PEO treatment because the electrolyte was under constant stirring.

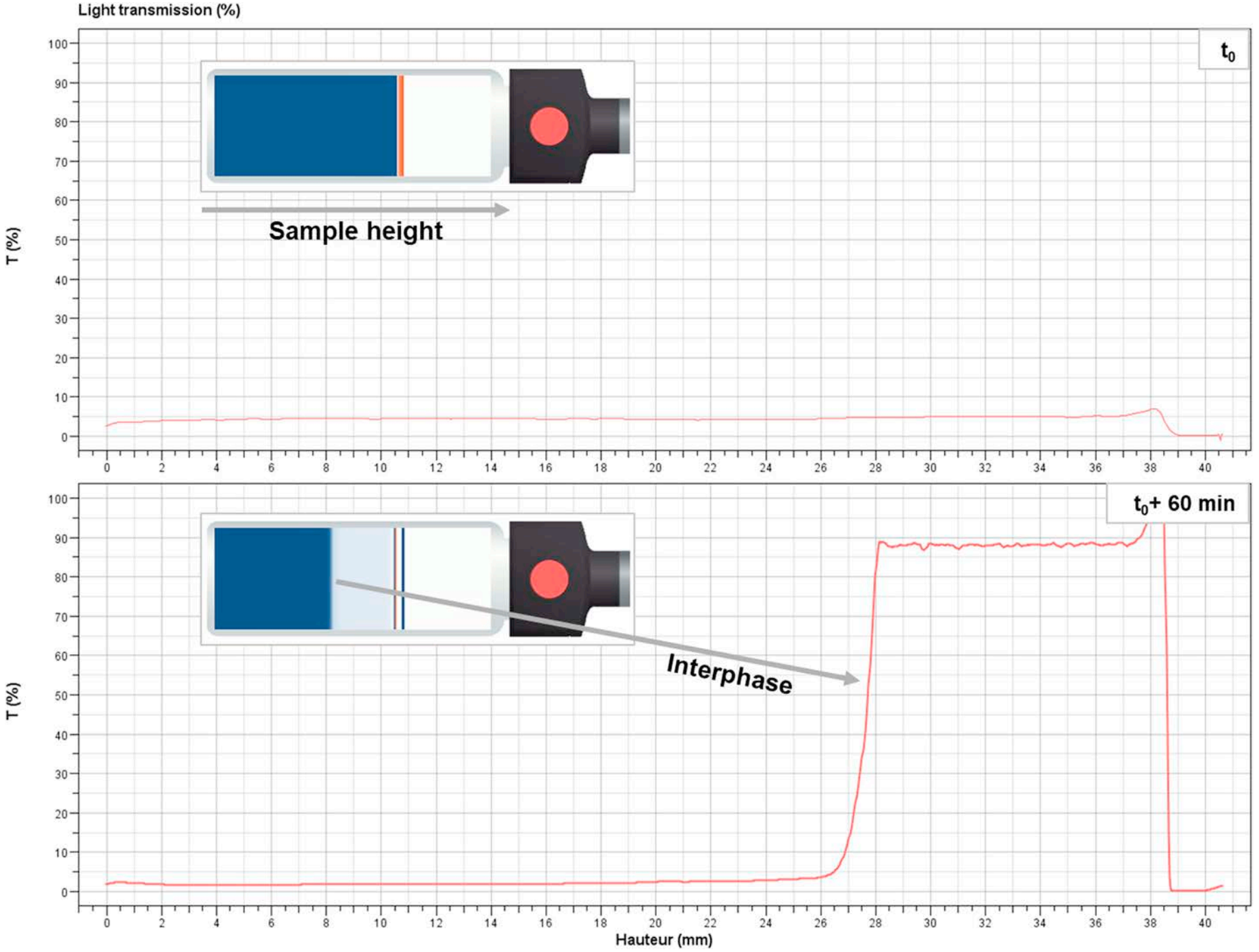

Fig. A.1. Evolution of light transmission through {KOH + Al + Si (C_1)} electrolyte after agitation (t_0) and after 60 min (t_0 + 60 min).

A.2. Gel characterizations

During the PEO treatment in {KOH + Al + Si (C_1)} electrolyte, a gel layer is also observed on TA6V surface, the gel amount increasing with treatment time. Solid state NMR analyses were performed (Fig. A.2) on the solid phase in this electrolyte before any PEO treatment. ^{29}Si NMR spectrum corresponds to two coordinations, on one hand one silicon atom coordinated with four aluminium atoms, and on the other hand silicon atom coordinated with three aluminium atoms and one silicon atom. Peaks on the ^{13}C spectrum (Fig. A.2), correspond to carbonate compounds in solution, induced by the incorporation of carbon dioxide initially present in ambient air.

Moreover, XRD was performed on powder resulting from the drying of the gel at 80 °C under air. Fig. A.3 shows an important amorphous phase (inset), but also crystallized KOH, SiO_2, Na_2CO_3, $K_6Si_3O_9$, $K_2Al_2Si_3O_{10}$. XRD results are in agreement with previous NMR results, but do not perfectly match the proposed compounds, calculated with PHREEQC software, i.e. β-Kalsilite ($KAlSiO_4$), Na-Phillipsite ($NaAlSi_3O_8{:}3H_2O$) and Analcime ($NaAlSi_2O_6{:}H_2O$). This difference could be probably explained by the drying step, inducing partial dehydration and precipitation modifications. To summarize, these characterizations show that the gel probably consist of amorphous silicon oxides (SiO_2…) and alumino-silicates compounds, formed by sol-gel process [24,25] in the electrolyte, composed of potash, aluminates and silicates. I. Krznaric et al. [26] described the gel skeleton as an aluminium atom in five-fold coordinated inside a complex network of aluminium, silicon and oxygen, neutrality being provided by sodium ion (Na^+) inside Al-O tetrahedral structure. This system is very stable and would explain that pH stayed unchanged (12.99 before any PEO treatment, 12.98 after 14 treatments) during PEO treatment.

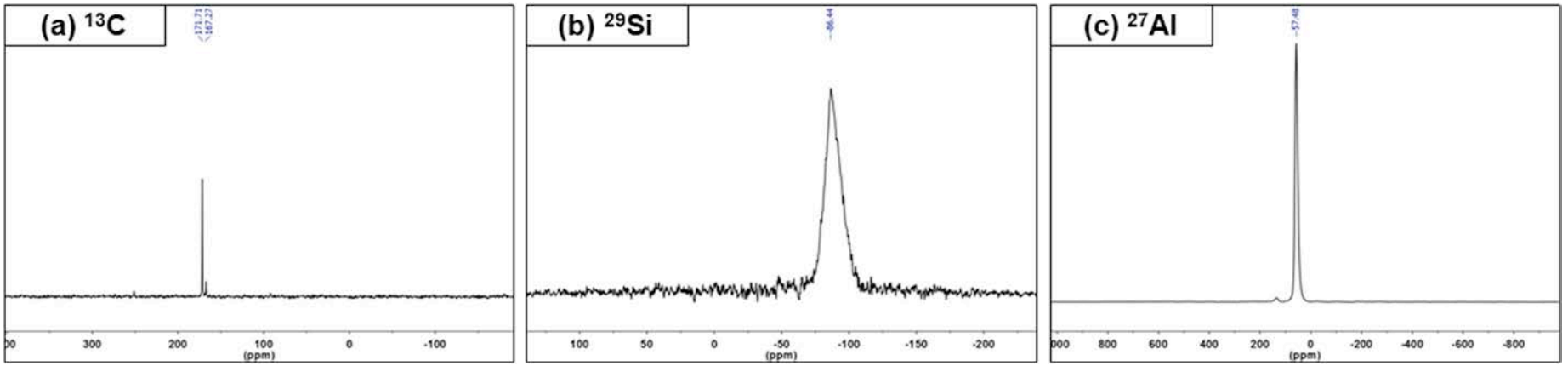

Fig. A.2. NMR spectra of ^{13}C, ^{29}Si and ^{27}Al in the gel identified in {KOH + Al + Si (C_1)} electrolyte.

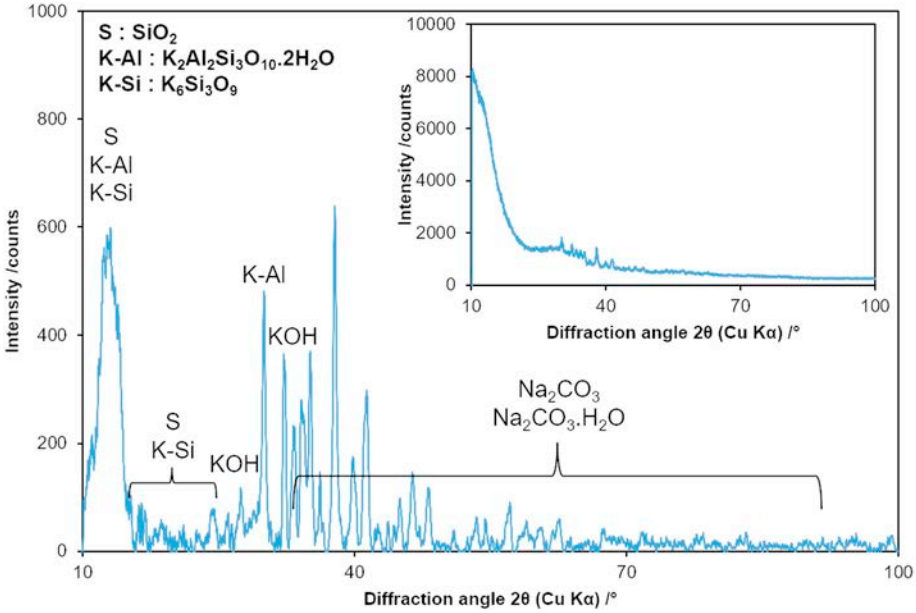

Fig. A.3. XRD pattern of the gel detected in {KOH + Al + Si (C_1)} electrolyte after drying at 80 °C; inset: raw XRD data of the dried gel.

References

[1] H. Habazaki, S. Tsunekawa, E. Tsuji, T. Nakayama, Formation and characterization of wear-resistant PEO coatings formed on β-titanium alloy at different electrolyte temperatures, Appl. Surf. Sci. 259 (2012) 711–718, https://doi.org/10.1016/j.apsusc.2012.07.104.

[2] A.L. Yerokhin, X. Nie, A. Leyland, A. Matthews, Characterisation of oxide films produced by plasma electrolytic oxidation of a Ti–6Al–4V alloy, Surf. Coat. Technol. 130 (2000) 195–206, https://doi.org/10.1016/S0257-8972(00)00719-2.

[3] Q. Li, W. Yang, C. Liu, D. Wang, J. Liang, Correlations between the growth mechanism and properties of micro-arc oxidation coatings on titanium alloy: effects of electrolytes, Surf. Coat. Technol. 316 (2017) 162–170, https://doi.org/10.1016/j.surfcoat.2017.03.021.

[4] S. Aliasghari, P. Skeldon, G.E. Thompson, Plasma electrolytic oxidation of titanium in a phosphate/silicate electrolyte and tribological performance of the coatings, Appl. Surf. Sci. 316 (2014) 463–476, https://doi.org/10.1016/j.apsusc.2014.08.037.

[5] Y. Wang, T. Lei, L. Guo, B. Jiang, Fretting wear behaviour of microarc oxidation coatings formed on titanium alloy against steel in unlubrication and oil lubrication, Appl. Surf. Sci. 252 (2006) 8113–8120, https://doi.org/10.1016/j.apsusc.2005.10.032.

[6] X.T. Sun, C.X. Lin, Tribological behaviour of ceramic coatings formed on titanium alloy through miro-arc oxidation technique, Key Eng. Mater. 353–358 (2007) 898–901, https://doi.org/10.4028/www.scientific.net/KEM.353-358.898.

[7] D. Dzhurinskiy, Y. Gao, W.-K. Yeung, E. Strumban, V. Leshchinsky, P.-J. Chu, A. Matthews, A. Yerokhin, R.G. Maev, Characterization and corrosion evaluation of TiO_2:n-HA coatings on titanium alloy formed by plasma electrolytic oxidation, Surf. Coat. Technol. 269 (2015) 258–265, https://doi.org/10.1016/j.surfcoat.2015.01.022.

[8] A.L. Yerokhin, A. Leyland, A. Matthews, Kinetic aspects of aluminium titanate layer formation on titanium alloys by plasma electrolytic oxidation, Appl. Surf. Sci. 200 (2002) 172–184, https://doi.org/10.1016/S0169-4332(02)00848-6.

[9] W. Xue, C. Wang, R. Chen, Z. Deng, Structure and properties characterization of ceramic coatings produced on Ti–6Al–4V alloy by microarc oxidation in aluminate solution, Mater. Lett. 52 (2002) 435–441, https://doi.org/10.1016/S0167-577X(01)00440-2.

[10] Y.M. Wang, B.L. Jiang, L.X. Guo, T.C. Lei, Controlled synthesis of microarc oxidation coating on Ti6Al4V alloy and its antifriction properties, Mater. Sci. Technol. 20 (2004) 1590–1594, https://doi.org/10.1179/026708304225019669.

[11] O. Banakh, T. Journot, P.A. Gay, J. Matthey, C. Csefalvay, O. Kalinichenko, O. Sereda, M. Moussa, S. Durual, L. Snizhko, Synthesis by anodic-spark deposition of Ca- and P-containing films on pure titanium and their biological response, Appl. Surf. Sci. 378 (2016) 207–215, https://doi.org/10.1016/j.apsusc.2016.03.161.

[12] M. Khorasanian, A. Dehghan, M.H. Shariat, M.E. Bahrololoom, S. Javadpour, Microstructure and wear resistance of oxide coatings on Ti–6Al–4V produced by plasma electrolytic oxidation in an inexpensive electrolyte, Surf. Coat. Technol. 206 (2011) 1495–1502, https://doi.org/10.1016/j.surfcoat.2011.09.038.

[13] S.R. Charlton, D.L. Parkhurst, Modules based on the geochemical model PHREEQC for use in scripting and programming languages, Comput. Geosci. 37 (2011) 1653–1663, https://doi.org/10.1016/j.cageo.2011.02.005.

[14] P. Blanc, A. Lassin, P. Piantone, M. Azaroual, N. Jacquemet, A. Fabbri, E.C. Gaucher, Thermoddem: a geochemical database focused on low temperature water/rock interactions and waste materials, Appl. Geochem. 27 (2012) 2107–2116, https://doi.org/10.1016/j.apgeochem.2012.06.002.

[15] C.W. Bale, E. Bélisle, P. Chartrand, S.A. Decterov, G. Eriksson, A.E. Gheribi, K. Hack, I.H. Jung, Y.B. Kang, J. Melançon, A.D. Pelton, S. Petersen, C. Robelin, J. Sangster, P. Spencer, M.A. Van Ende, FactSage thermochemical software and databases, 2010–2016, Calphad 55 (2016) 1–19, https://doi.org/10.1016/j.calphad.2016.07.004.

[16] I.-H. Jung, G. Eriksson, P. Wu, A. Pelton, Thermodynamic modeling of the Al_2O_3-Ti_2O_3-TiO_2 system and its applications to the Fe-Al-Ti-O inclusion diagram, ISIJ Int. 49 (2009) 1290–1297, https://doi.org/10.1063/1.2822460.

[17] Y.B. Kang, I.H. Jung, H.G. Lee, Critical thermodynamic evaluation and optimization of the MnO-SiO_2-"TiO_2"-"Ti_2O_3" system, Calphad 30 (2006) 226–234, https://doi.org/10.1111/j.1600-051X.2006.00893.x.

[18] S.J. Smith, R. Stevens, S. Liu, G. Li, A. Navrotsky, J. Boerio-Goates, B.F. Woodfield, Heat capacities and thermodynamic functions of TiO_2 anatase and rutile: analysis of phase stability, Am. Mineral. 94 (2009) 236–243, https://doi.org/10.2138/am.2009.3050.

[19] M. Pourbaix, Atlas of Electrochemical Equilibria National in Aqueous Solution, second ed., National Association of Corrosion Engineers, Ann Arbor, 1974.

[20] J. Xiang Han, Y. Lin Cheng, W. Bin Tu, T.Y. Zhan, Y. Liang Cheng, The black and white coatings on Ti-6Al-4V alloy or pure titanium by plasma electrolytic oxidation in concentrated silicate electrolyte, Appl. Surf. Sci. 428 (2018) 684–697, https://doi.org/10.1016/j.apsusc.2017.09.109.

[21] M.D. Allendorf, K.E. Spear, Thermodynamic analysis of silica refractory corrosion in glass-melting furnaces, J. Electrochem. Soc. 148 (2001) B59–B67, https://doi.org/10.1149/1.1337603.

[22] N.N. Greenwood, A. Earnshaw, Silicon, in: Butterworth-Heinemann (Ed.), Chemistry of the Elements, 1997, pp. 328–366 (Oxford).

[23] X.-J. Li, G.-A. Cheng, W.-B. Xue, R.-T. Zheng, Y.-J. Cheng, Wear and corrosion resistant coatings formed by microarc oxidation on TiAl alloy, Mater. Chem. Phys. 107 (2008) 148–152, https://doi.org/10.1016/j.matchemphys.2007.06.067.

[24] M. Hunger, Solid-state NMR spectroscopy, in: A.W. Chester, E.G. Derouane (Eds.), Zeolite Characterization and Catalysis, Springer Science, Berlin, 2009, pp. 65–103.

[25] I. Krznarić, T. Antonić, B. Subotić, Physical chemistry of aluminosilicate gels. Part 1. Influence of batch concentration on chemical composition of the gels, Zeolites 19 (1997) 29–40, https://doi.org/10.1016/S0144-2449(97)00049-3.

[26] I. Krznarić, T. Antonić, B. Subotić, Physical chemistry of aluminosilicate gels. Part 2 influence of the batch molar ratio SiO_2/Al_2O_3 on chemical composition of the gels, Microporous Mesoporous Mater. 20 (1998) 161–175, https://doi.org/10.1016/S1387-1811(97)00010-3.